Spin glasses on the hypercube

L. A. Fernández,[1,2] V. Martin-Mayor,[1,2] G. Parisi,[3] and B. Seoane[1,2]

[1]*Departamento de Física Teórica I, Universidad Complutense, 28040 Madrid, Spain*
[2]*Instituto de Biocomputación y Física de Sistemas Complejos (BIFI), Zaragoza, Spain*
[3]*Dipartimento di Fisica, INFM-CNR (SMC), Università di Roma "La Sapienza," 00185 Roma, Italy*

We present a mean field model for spin glasses with a natural notion of distance built in, namely, the Edwards-Anderson model on the diluted D-dimensional unit hypercube in the limit of large D. We show that finite D effects are strongly dependent on the connectivity, being much smaller for a fixed coordination number. We solve the nontrivial problem of generating these lattices. Afterward, we numerically study the nonequilibrium dynamics of the mean field spin glass. Our three main findings are the following: (i) the dynamics is ruled by an infinite number of time sectors, (ii) the aging dynamics consists of the growth of coherent domains with a nonvanishing surface-volume ratio, and (iii) the propagator in Fourier space follows the p^4 law. We study as well the finite D effects in the nonequilibrium dynamics, finding that a naive finite size scaling ansatz works surprisingly well.

I. INTRODUCTION

Spin glasses (SGs) are highly disordered magnetic systems.[1] Rather than by their practical usefulness, SGs are often studied as a paradigmatic example of a complex system. Indeed, they display an extremely slow dynamics on a complex free-energy landscape with many degenerate states. In addition, SGs are a convenient experimental model for glassy behavior due to the comparatively fast microscopic spin dynamics as compared, for instance, with supercooled liquids. In fact, nowadays, SGs are considered as a playground to learn about general glassy behavior, biology, financial markets, minimization problems in computer science, etc.

Maybe the most conspicuous feature of SGs is *aging*: they never reach thermal equilibrium in experimental times. Here we will only consider the simplest possible experimental protocol, the temperature quench (see Ref. 2 for very interesting and more sophisticated experimental procedures): the sample is cooled below the critical temperature, T_c, and it is let to relax for a time t_w at the working temperature T. Its properties are studied at a later time $t+t_w$. It turns out that, if a magnetic field was applied from the temperature quench until t_w, when it is switched off, the thermoremanent magnetization $M(t,t_w)$ decays with t/t_w [at least for $10^{-3} < t/t_w < 10$ and 50 s $< t_w < 10^4$ s (Ref. 3)]. This lack of a characteristic time beyond t_w, the glassy system age, is known as *full aging*. We now know that full aging is an effective description of the dynamics, no longer valid for $t/t_w \sim 10^4$ and $t_w \sim 10$ s.[4]

Nowadays, we know that the slow dynamics in SGs is due to a thermodynamic phase transition at T_c.[5] Below T_c, the spins associate in coherent domains whose size, $\xi(t_w)$, grows with time. The lower the temperature is, the slower the growth of $\xi(t_w)$ is [experimentally, $\xi(t_w=100$ s; $T=0.9T_c)$ ~ 100 atomic spacings].

There is a lively theoretical debate on the properties of the low temperature phase. Surprisingly enough, this controversy on the equilibrium properties of a nonaccessible (in

human time scales) spin-glass phase is relevant to *nonequilibrium* experiments.[6] In fact, it has been recently shown[7,8] that there is a quantitative correspondence between the nonequilibrium spatial correlation functions and the equilibrium ones (in the $q=0$ sector).

Mainly, there are two competing theories: the *droplets*[9] and the replica symmetry breaking (RSB).[10] According to the droplets' picture, the SG phase would be ferromagneticlike, with a complicated spin texture but essentially with only two equilibrium states. On the other hand, the RSB theory predicts an infinite number of degenerated states with an ultrametric organization. For both theories, aging would be a coarsening process in the sense that coherent domains of low temperature phase grow with time. The two theories disagree in their predictions for these domain properties. According to the droplets, the domains would be compact objects with a surface-volume ratio that vanishes in the high $\xi(t_w)$ limit.[11] The SG order parameter is nonzero inside of each domain. On the contrary, the RSB theory expects noncompact domains with a surface-volume ratio constant for large $\xi(t_w)$. Furthermore, in a RSB system, the SG order parameter vanishes inside those domains. In recent times, a somehow intermediate theory *trivial-nontrivial* has been proposed,[12] but, to our knowledge, no detailed dynamic predictions have been provided.

The RSB theory is based on the mean field (MF) approximation which, unlike in the ferromagnetic case, is highly nontrivial. Indeed, after 30 years of study, aging is not yet fully understood, not even within MF approximations. Therefore, nonperturbative tools, such as Monte Carlo (MC) calculations, appear as an appealing alternative. Furthermore, MC calculations are called for even at the MF level. Hence, one is interested in mean field models, that is to say models where the MF approximation becomes exact in the thermodynamic limit (TL). The standard MF model [the Sherrington-Kirkpatrick (SK) model (see Ref. 13 and Sec. II)] has a number of disadvantages. It lacks a natural notion of distance [hence one cannot discuss a coherence length $\xi(t_w)$] or coordination number. Furthermore, its numerical simulation is computationally heavy. In fact, recent advances

on the analytical study of spin glasses on the Bethe lattices[14] have shifted the attention to these far more numerically tractable models which share with experimental systems the notion of a coordination number.

Here we present a MF model for spin glasses: the spin glass on a D-dimensional hypercube with *fixed* connectivity.[15] In the thermodynamic limit (which coincides with the large D limit for this model), the Bethe approximation becomes exact. As a consequence, the statics is of Bethe-lattice type and can be computed. A nice feature of this model is that it has a natural definition of distance, which allow us to study spatial correlations within MF approximation. In other words, this MF model is more similar to a real $D=3$ system than those considered previously since the space-time correlation functions can be studied. Our main results focus on the nonequilibrium dynamics (although we present some equilibrium results that we regard as useful consistency tests).

The structure of this paper will be the following. In Sec. II we will describe the model and compare it with other MF models. In particular, in Sec. IIA we will address the problem of fixing the connectivity in a diluted hypercube. In Sec. III we will briefly explain the numerical methods we have used and in Sec. IV we will introduce the observables measured during the simulations. In Secs. V and VI, the numerical results will be presented both in equilibrium (as a test of the model) and nonequilibrium, respectively. In Sec. VII we will discuss finite size effects. The analysis will reveal the p^4 propagator,[16] long sought in numerical investigations. Our conclusions will be presented in Sec. VIII. Finally, we include extended discussions in Appendixes A and B.

II. MODELS

The standard model in SGs is the Edwards-Anderson (EA) model. We will work with two kinds of degrees of freedom: dynamical and quenched. The dynamical ones correspond to the spins, σ_i, with $i=1,2,\ldots,N$. We will consider them as Ising variables, ± 1. The nondynamical (or quenched) ones represent the material impurities. We will consider here two types of them: the connectivity matrix, $n_{ik}=n_{ki}=1,0$ ($n_{ik}=1$ as long as spins i and k interact), and the coupling constants, $J_{ik}=J_{ki}$, which shall take only two opposite values (in general with certain exceptions that will be discussed in the next paragraph, we will consider $J_{ik}=\pm 1$, which defines our energy scale). The interaction energy is

$$\mathcal{H} = -\sum_{i<k} J_{ik} n_{ik} \sigma_i \sigma_k. \qquad (1)$$

Since the impurity diffusion time is huge compared to the *spin flip* (picosecond), we will always work within the so-called quenched approximation: spins cannot have any kind of influence over the material impurities. Then, both the set of coupling constants in the Hamiltonian and its associated Gibbs free energy will be considered random variables. Therefore, in order to rationalize the experiments, the useful free energy will be an average over the disorder. We will refer to each assignment of $\{n_{ik}, J_{ik}\}$ as a *sample*. Its probability distribution defines the actual EA model. The average over samples will be represented as $\overline{(\cdots)}$.

Only a few exact results are known for Hamiltonian (1) and all them were obtained within the MF approximation.[10] This *approximation* becomes exact in a weak infinite-range interaction model (in a ferromagnet $n_{ik}=1$ and $J_{ik}=1/N$ for each couple i,k). In SGs it is usually represented as $n_{ik}=1$ for every couple i,k and, because of the random ferromagnetic and antiferromagnetic interaction characters, $\{J_{ik}\}$ are independent Gaussian random variables, with zero mean and variance $1/N$.[13]

Computer simulations of long-range models are extremely hard because the energy evaluation for a system of N spins requires N^2 operations. The situation has improved since the discovery that EA models on the Bethe lattices (not to be confused with the Bethe trees) undergo replica symmetry breaking at T_c.[14]

A very popular realization of a Bethe-lattice spin glass is the EA model on a Erdos-Renyi graph. A simple way of drawing one of these graphs consists of connecting ($n_{ik}=1$) each possible pair of spins, i,k [there are $N(N-1)/2$ possible couples], with probability $z/(N-1)$. Thus, the number of neighbors of spin i, its coordination number n_i, follows in the large-N limit a Poisson distribution function with average z (the connectivity). We will consider $z=6$ to mimic a three-dimensional (3D) system. These kinds of graphs are locally cycleless: the mean shortest length among all the closed loops that passes through a given point is $O(\log N)$, i.e., the system is still locally treelike. Computationally convenient as they are, the Erdos-Renyi graphs still lack a natural notion of distance.

A simple alternative consists of formulating the model on a D-dimensional unit hypercube. Thus, the spins are located in each of the hypercube vertices (then, $N=2^D$) and the bonds lie on the edges. Therefore, each spin can be connected with, at most, $D=\log_2 N$ spins. In analogy with the Poissonian graph, we consider that a link is active (i.e., $n_{ik}=1$) over each edge with probability z/D. We call this model *random-connectivity hypercube*. It is easy to prove that it is locally treelike as well: the density of closed loops of length l decays, at least, with D^{-2} (i.e., with the squared logarithm of N, as it also happens in the Erdos-Renyi graph). Incidentally, one could consider as well a nondiluted hypercube, but this would have two shortcomings: the connection with three-dimensional systems would get lost and the numerical simulation would become computationally heavy for large D.

Note that, at variance with other infinite-dimensional graphs, the hypercube has at least two natural notions of distance: the Euclidean metrics and the postman metrics. In the postman metrics, the distance between two points, $\boldsymbol{x}$ and $\boldsymbol{y}$, is given by the minimum number of edges, either occupied or not, which must be covered when joining $\boldsymbol{x}$ and $\boldsymbol{y}$. The two distances are essentially equivalent since the Euclidean distance between two sites in the hypercube is merely the square root of the postman distance.

In the following we shall use the postman metrics, which has some amusing consequences. For instance, our correlation length will be the *square* of the Euclidean one, thus yielding a critical exponent $\nu=1$, doubling the expected $\nu_{MF}=1/2$. Of course, if we use the Euclidean metric we recover the usual exponent $\nu=1/2$.

However, it turns out that the random-connectivity hypercube suffers a major disadvantage. The inverse of the critical temperature in a ferromagnet[17] or in a SG[18] can be computed within the Bethe approximation,

$$K_c^{FM} = \text{arctanh} \frac{1}{\langle n \rangle_1 - 1}, \quad K_c^{SG} = \text{arctanh} \frac{1}{\sqrt{\langle n \rangle_1 - 1}}. \quad (2)$$

In this expression $\langle n \rangle_1$ is a conditional expectation value for n, the coordination number of a given site in the graph. This conditional expectation value is computed knowing for sure that our site is connected to another *specific* site (this is different from the average number of neighbors of a site that has at least one neighbor). A simple calculation shows that $\langle n \rangle_1 = 1 + z - \frac{z}{D}$ in the random-connectivity model. Since $D = \log_2 N$, we must expect huge finite size corrections $[O(1/\log N)]$ at the critical point. Note that this problem is far less dramatic for a Erdos-Renyi graph where $\langle n \rangle_1 = 1 + z - \frac{z}{N-1}$.

The cure seems rather obvious: place the occupied links in the hypercube in such a way that $n = z$ (here, $z = 6$). Unfortunately, drawing these graphs poses a nontrivial problem in computer science.[19] Our solution to this problem is discussed in the next section.

Fixed connectivity hypercube

We have not found any systematic way of activating links in the hypercube that respects the fixed connectivity condition. Thus, we have adopted an operational approach: the distribution of bonds is obtained by means of a dynamic MC. We must define a MC procedure that generates a set of graphs that remains invariant under all symmetry transformations of the hypercube group.

Specifically, we start with an initial condition in which all bonds along the directions one to six are activated (of course, this procedure makes sense only for $D \geq 6$). Clearly enough, the initial condition verifies the constraint $n = 6$. We shall modify the bond distribution by means of movements that do not change n. We perform what we called a "plaquette" transformation (a plaquette is the shortest possible loop in the hypercube, of length 4). We randomly pick, with uniform probability, one hypercube plaquette. In case this plaquette contains only two parallel active links ($n_{ik} = 1$), these two links are deactivated at the same time that the other two are activated. On the opposite case, nothing is done.[20] This guarantees that the set of generated graphs is isotropic.

In order for this procedure to be useful, the dynamic MC correlation times must be short. In Fig. 1, we show the MC evolution of the system isotropy. We make kN plaquette transformations, and we control the density of occupied bonds in two directions: the first direction (initially occupied in every vertex) and the seventh direction (initially unoccupied). As we see, for two different system sizes, we get short isotropization exponential times (for $D = 22$ we get $\tau_{exp} \approx 4.7N$). For this reason, we assume that taking $k = 100$ is long enough to ensure that the configurations obtained are completely independent from the initial condition.

At this point, the question arises of the completeness of the generated set of graphs. We first note that our set contains
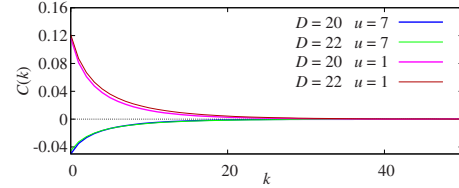

FIG. 1. (Color online) Generation algorithm of fixed connectivity graphs: for two system sizes ($D = 20, 22$) and two spatial directions ($u = 1, 7$), we represent the density of occupied edges as a function of the MC time. As MC time goes on, the system recovers the lost isotropy induced by the initial condition.

proper subsets that are also isotropic. However, finding them would require more involved algorithms which will not pay in a reduction of statistical errors (as we will show below, most of the sample dispersion is induced by the coupling matrix $\{J_{ik}\}$). On the other hand, one could think that there are lacking graphs in our algorithm for a simple reason. The plaquette transformation cannot break loops: when we interchange neighboring links we can only either join two different loops or split up a loop into two loops. Due to the hypercube boundary conditions, in the initial configuration all sites belonged to closed loops. This situation cannot be changed by plaquette transformations. However, this objection does not resist a close inspection. In fact, a nonclosed lattice path formed by occupied links should have an ending point with an *odd* coordination number, which violates the constraint $n = z$ for any even z. Thus, all lattice paths compatible with our fixed connectivity constraint do form closed loops. This argument, as well as the numerical checks reported below, makes us confident that the set of generated graphs is general enough for our purposes. Actually, we conjecture that our algorithm generates *all* possible fixed connectivity graphs with z even.

One may worry as well about the applicability of the Bethe approximation to the fixed connectivity model since all loops are closed. Actually, the crucial point to apply the Bethe approximation is that the probability of having a closed path of any *fixed* length should vanish in the large D limit. This is easy to prove for the random-connectivity model. In the fixed connectivity case, one may argue as follows. Let us imagine a walk over the closed path. On the very first step, the probability that the chosen link is present is z/D, whereas in the following step the probability of finding the link is $(z-1)/(D-1)$ in the limit of large D (since one of the z links available at the present site was already used to get there). This estimate implicitly assumes that the occupancy of different links is statistically independent. The independency approximately holds for large D and becomes exact in the $D \to \infty$ limit, where occupied links form a diluted set. At this point, the estimate of the number of paths of any given fixed length in the large D limit can be performed as in the random-connectivity case. One finds as well, in the fixed connectivity case, that the number of closed loops of a given length per site decays at least as $O(1/D^2)$.

In addition to the above considerations, we may numerically compute in our graphs the length of the second shortest path that joins two *connected* nearest neighbors in the hypercube. In Fig. 2, we compare the probabilities for the length
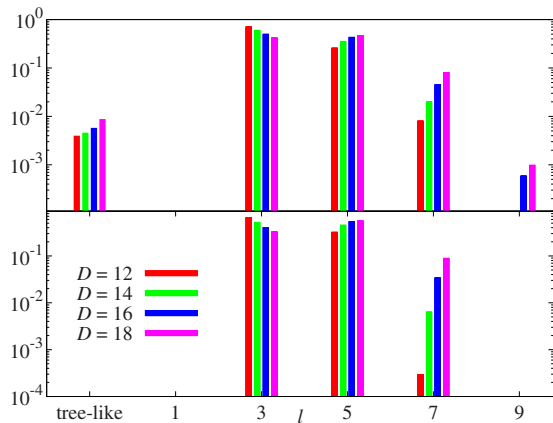
FIG. 2. (Color online) For (top) random-z graphs and (bottom) fixed z for plaquette transformations, the probability distribution function of the length of the second shortest path joining nearest neighbors for several $N=2^D$ (mind the vertical axis is in logarithmic scale). Lines have been slightly displaced in order to help the visualization.

of such paths in the random (top) and fixed (bottom) connectivity models for different system sizes.[21] In both cases, we note that the maximum of the probability shifts to larger length as D grows. We note as well that, for fixed connectivity, no treelike graph arises.[22]

A summary of our efforts is shown in Fig. 3, where we plot the dependency of the critical point with D for the ferromagnetic Ising model, defined on hypercubes with both random and fixed connectivities. As expected, the random-connectivity model suffers very important finite volume corrections which make it essentially useless for numerical studies. The problem is solved using fixed connectivity hypercubes instead, where the finite volume effects are only caused by the residual presence of short closed loops.

III. NUMERICAL METHODS

We have simulated Hamiltonian (1) using a Metropolis algorithm.[23] In addition, we use *multispin coding*: since spins are binary variables, we can simultaneously codify 64 sys-
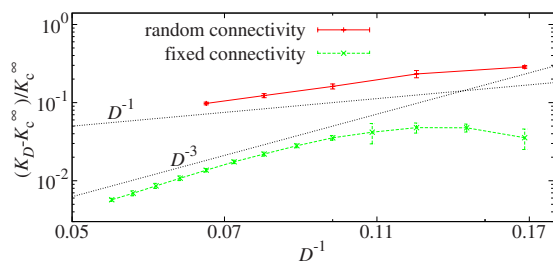

FIG. 3. (Color online) Comparison of finite volume effects in the critical point estimators K_c^D for ferromagnetic Ising model both in the random (red dots) and fixed (green crosses) connectivity hypercubes. As a guide for the eyes, we have included two different scalings with D. The estimator K_c^D corresponds to the average of the inverse temperatures at which Binder cumulant (7) reaches the values 1.2 and 2.4.

tems in one single 64 bits word (all of them share the same connectivity matrix, n_{ik}). With this common matrix, we find errors which are approximately seven times smaller than those obtained with one single sample per matrix. This should be compared with the factor 8 that we would obtain in case no correlation was induced. Our program needs 0.29 ns/spin flip in an Intel i7 at 2.93 GHz (in Ref. 24 Hasenbusch *et al.* reported ~1.2 ns/spin flip on an Opteron at 2.0 GHz, for the simulation of the $D=3$ EA model in the cubic lattice).

In a nonequilibrium dynamical study such as ours, one computes both one-time and two-time quantities (see Sec. IV). The calculation of two-time quantities implies the storage on disk of intermediate configurations. Disk capacity turned out to be the main limiting factor for the simulation. For this reason, we have worked in parallel with two program versions: one valid for measuring quantities at one and two times and another restricted to the computation of one-time quantities.

We have computed two-time quantities at temperature $T=0.7T_c$ on systems with $D=16$, 18, 20, and 22. The numbers of simulated samples were 8×64 samples for each system size (hence, for self-averaging quantities the statistical quality of our data grow with D).

Besides, up to our knowledge, an EA model has not been studied before in the fixed connectivity hypercube. Intensive testing is therefore mandatory. This is why we have computed *equilibrium* one-time quantities at $T/T_c=0.95$, 0.97, 0.99, 1, 1.1, 1.2, 1.3, and 1.4. The system sizes were again $D=16$, 18, 20, and 22. The numbers of simulated samples were 128×64 samples per temperature (at T_c we computed 256×64 samples).

IV. OBSERVABLES

Hamiltonian (1) has a global symmetry $\mathbb{Z}_2$ ($\sigma_i \rightarrow -\sigma_i$ for all i). Not as obvious is the gauge symmetry induced by the average over couplings. In fact, choosing randomly a sign for each position, $\varepsilon_i = \pm 1$, energy (1) is invariant under the transformation

$$\sigma_i \rightarrow \varepsilon_i \sigma_i, \quad J_{ik} \rightarrow \varepsilon_i \varepsilon_k J_{ik}. \quad (3)$$

Now, since the transformed couplings $\varepsilon_i \varepsilon_k J_{ik}$ are just as probable as the original ones, we need to define observables that are invariant under gauge transformation (3). With this aim we form gauge invariant fields from two systems at equal time, which evolve independently with the same couplings, $\{\sigma_i^{(1)}, \sigma_i^{(2)}\}$ (real replicas), or, alternatively, from a single system considered at two different times,

$$q_i(t_w) = \sigma_i^{(1)}(t_w) \sigma_i^{(2)}(t_w),$$

$$c_i(t,t_w) = \sigma_i^{(1)}(t+t_w) \sigma_i^{(1)}(t_w). \quad (4)$$

In the following sections, we define three kinds of quantities using both fields, as well as the Fourier transform in our peculiar geometry.

A. One-time quantities

The order parameter

$$q(t_w) = \frac{1}{N} \sum_i q_i(t_w) \qquad (5)$$

vanishes in the nonequilibrium regime [the system is much bigger than the coherence length, $\xi(t_w)$]. We define the SG susceptibility as

$$\chi_{SG}(t_w) = N \overline{q^2(t_w)}. \qquad (6)$$

The long t_w limit of $\chi_{SG}(t_w)$ is proportional to the nonlinear magnetic susceptibility but only in the paramagnetic phase. In the SG phase, for an infinite system, χ_{SG} grows with t_w without bound [in fact, as a power of $\xi(t_w)$].

The Binder parameter provides us with information about the fluctuations,

$$B(t_w) = \frac{\overline{q^4(t_w)}}{\overline{q^2(t_w)}^2}. \qquad (7)$$

In the Gaussian regime $B = 3$. In a ferromagnetic phase, $B = 1$. In the SG phase, the long time limit and the infinite size limit do not commute. If one takes first the thermodynamic limit, one stays forever in the $q = 0$ sector of the nonequilibrium dynamics. In this regime $B = 3$ since the fluctuations are Gaussian. On the other hand, if one takes before the limit of long t_w, thermal equilibrium is reached. B grows with the temperature from $B = 1$ at $T = 0$. The equilibrium paramagnetic phase is in Gaussian regime.

B. Two-time quantities

The correlation spin function tells us about the memory kept by the system at time $t + t_w$, about the configuration at t_w,[25]

$$C(t, t_w) = \frac{1}{N} \overline{\sum_i c_i(t, t_w)}. \qquad (8)$$

The susceptibility is $\chi(\omega = 2\pi/t, t_w) \propto [1 - C(t, t_w)]/T$.[26] On the other hand, when t_w is fixed, $C(t, t_w)$ is just the thermoremanent magnetization.[27]

The link correlation function

$$C_{link}(t, t_w) = \frac{1}{zN} \overline{\sum_{ik} n_{ik} c_i(t, t_w) c_k(t, t_w)} \qquad (9)$$

carries the information of the density of the interfaces between coherent domains at t_w, which at $t + t_w$ have flipped. In case the surface-volume ratio decayed with a negative power of $\xi(t_w)$ (droplets), C_{link} would become t independent.[28] On the contrary, in a RSB system, $C_{link} = a + bC^2$. Note that, for the Sherrington-Kirkpatrick model, one trivially finds $C_{link} = C^2$, but the linear relation is not straightforward in fixed connectivity mean field models.

C. Spatial correlation functions

In the unit hypercube, the binary decomposition of the spin index $i = 1, 2, \ldots, 2^D$ can be identified with its Euclidean coordinates, $\boldsymbol{x}$. The spatial correlation function is
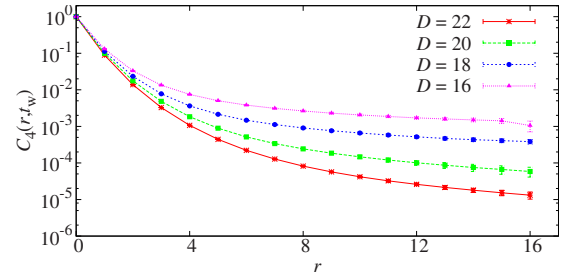

FIG. 4. (Color online) $C_4(r, t_w)$ [Eq. (11)] for $t_w = 2^8$ and different system sizes, $N = 2^D$, at $T = 0.7 T_c$.

$$c_4(\boldsymbol{r}, t_w) = \frac{1}{N} \overline{\sum_{\boldsymbol{x}} q_{\boldsymbol{x}}(t_w) q_{\boldsymbol{x}+\boldsymbol{r}}(t_w)}. \qquad (10)$$

We consider $r = |\boldsymbol{r}|$ as the distance in the postman metrics. It would look rather natural to average all the $c_4(\boldsymbol{r}, t_w)$ over the $N_r = \binom{D}{r}$ displacements of length $r = |\boldsymbol{r}|$,

$$C_4(r, t_w) = \frac{1}{N_r} \sum_{\boldsymbol{r}, |\boldsymbol{r}| = r} c_4(\boldsymbol{r}, t_w). \qquad (11)$$

However (see Fig. 4), $C_4(r, t_w)$ does not present a limiting behavior with D for a given t_w.

We can get a clue by looking at $\chi_{SG}(t_w)$ (Fig. 5), which does reach a thermodynamic limit. Since $\chi_{SG}(t_w)$ is nothing but the integral of $C_4(r, t_w)$ with the Jacobian $\binom{D}{r}$, it seems reasonable to define the following spatial correlation function instead:

$$\hat{C}_4(r, t_w) = \sum_{\boldsymbol{r}, |\boldsymbol{r}| = r} c_4(\boldsymbol{r}, t_w). \qquad (12)$$

We can see that $\hat{C}_4(r, t_w)$ does reach the high-D limit (Fig. 6) at least for short t_w. Besides, in the paramagnetic phase, it is possible to compute analytically $\hat{C}_4(r, t_w)$ (see Appendix A), taking first the limit $t_w \to \infty$ and making afterward $D \to \infty$. The resulting correlation function, which is only valid in the paramagnetic phase, is a simple exponential. Hence, both the equilibrium and the nonequilibrium computations suggest that one should focus on $\hat{C}_4$ rather than on C_4.

We note in Fig. 6 that, in the SG phase, $\hat{C}_4$ is nonmonotonically decreasing with r but rather presents a maximum. This maximum moves to bigger r with t_w; then, the system has a characteristic length that increases with time.
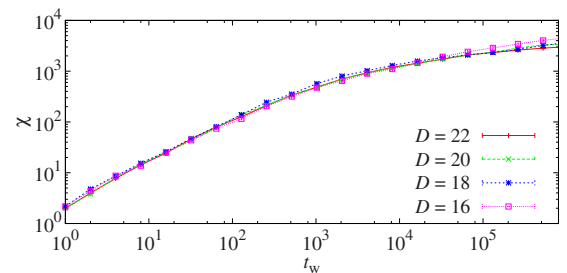

FIG. 5. (Color online) SG susceptibility a $T = 0.7 T_c$ as a function of t_w for different system sizes, $N = 2^D$.
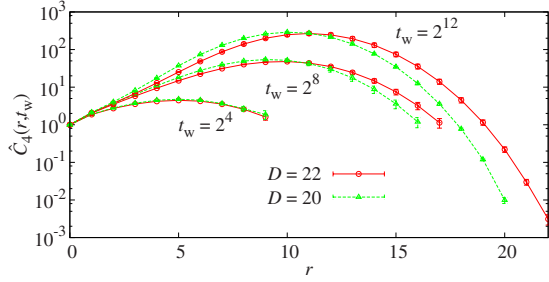
FIG. 6. (Color online) $\hat{C}_4(r,t_w)$ [Eq. (12)] for $D=10$ and 22 for $t_w=2^4$, 2^8, and 2^{12} at $T=0.7T_c$. This has to be compared with the behavior of $C_4(r,t_w)$ (Fig. 4).

Thus, we can estimate the coherence length by means of the integral estimator $\xi_{0,1}(t_w)$,

$$\xi_{0,1}(t_w) = \frac{\int_0^\infty dr\, r\hat{C}_4(r,t_w)}{\int_0^\infty dr\, \hat{C}_4(r,t_w)}. \tag{13}$$

A major advantage of $\xi_{0,1}$ over more heuristic definitions of the coherence length is that it is computed from self-averaging quantities (see details in Refs. 7 and 28; we note that, in this work, we have not tried to estimate the contribution to the integrals by the noise-induced long distance cutoff). The existence of such a characteristic length is the main advantage of the hypercube model over other MF models.

D. Correlation functions in the Fourier space

We define the Fourier transform in the standard way. Our wave vectors are $\boldsymbol{k}=\pi(n_1,n_2,\ldots,n_D)$ with $n_i=0,1$. The propagator is

$$G(\boldsymbol{k},t_w) = \sum_{\boldsymbol{r}} e^{i\boldsymbol{k}\cdot\boldsymbol{r}} c_4(\boldsymbol{r},t_w). \tag{14}$$

In particular, $G(0,t_w)=\Sigma_{r=0}^D \hat{C}_4(r,t_w)=\chi_{\text{SG}}(t_w)$.

Now, because of the disorder average, $c_4(\boldsymbol{r},t_w)$ is only a function of $r=|\boldsymbol{r}|$ (postman metrics). It follows from Eq. (17) that $G(\boldsymbol{k},t_w)$ actually depends only on $k=|\boldsymbol{k}|$.

The rotational invariance allows us for a major simplification[29] [with a slight abuse of notation, we write $c_4(r,t_w)$ rather than $c_4(\boldsymbol{r},t_w)$],

$$G(k,t_w) = \sum_{r=0}^D K_r(D,k) c_4(r,t_w), \tag{15}$$

where $K_r(D,k)$ are the *Krawtchouk polynomials*,

$$K_r(D,k) = \sum_{m=\max(0,r+k-D)}^{\min(k,r)} (-1)^m \binom{k}{m}\binom{D-k}{r-m}. \tag{16}$$

It is interesting to point out that neither $K_r(D,k)$ nor $c_4(r,t_w)$ has a thermodynamic limit, while $G(k,t_w)$ does so. In fact, when $k=0$, $K_r(D,0)=\binom{D}{r}$ is diverging. Thus, we can rewrite Eq. (15) in terms of quantities with a well-defined limit, i.e.,

TABLE I. Comparison between the SG susceptibility in large D limit for the paramagnetic phase [Eq. (18)] and numerical results for $D=20,22$.

T	$\chi(T)_{D=\infty}$	$\chi(T)_{D=20}$	$\chi(T)_{D=22}$
$1.4T_c$	2.4497…	2.41(3)	2.44(3)
$1.3T_c$	3.0176…	2.98(4)	2.98(4)
$1.2T_c$	4.1650…	4.08(6)	4.10(7)
$1.1T_c$	7.6344…	7.11(13)	7.43(11)
T_c	∞	26(2)	98(7)

$$G(k,t_w) = \sum_{r=0}^D \frac{K_r(D,k)}{\binom{D}{r}} \hat{C}_4(r,t_w). \tag{17}$$

V. EQUILIBRIUM RESULTS

Since an EA model on a fixed connectivity hypercube has not been studied before it is necessary to make a few consistency checks. Equilibrium results are most convenient in this respect since we have analytical computations (valid only for the large D limit) to compare with.

We will briefly study the spatial correlations in the paramagnetic phase. In addition, we will check, by approaching to T_c from the SG phase, that the SG transition does lie on the predicted T_c [Eq. (2)].

A. Paramagnetic phase

Our very first check will be the comparison between the Monte Carlo estimate of the SG susceptibility (at finite D) with the analytical computation for infinite D,

$$\chi(T) = 1 + \frac{z \tanh^2 T^{-1}}{1-(z-1)\tanh^2 T^{-1}} \tag{18}$$

(see Appendix A). Our results are presented in Table I. We see that finite size effects increase while approaching T_c. For our larger system, $D=22$, the susceptibility significantly deviates from the asymptotic result only in the range $T_c < T < 1.1T_c$.

After the fast convergence to the large D limit observed in the SG susceptibility, the results for $\hat{C}_4$ are a little bit disappointing. In Fig. 7 we display $\hat{C}_4(r,D)-\hat{C}_4(r,\infty)$ as a function of r. We can see that finite size effects become more important once one approaches T_c.

Besides, finite D corrections as a function of r oscillate between positive and negative values. This is not surprising: the finite D corrections to the susceptibility are very small and they are nothing but the integral under these curves. More quantitatively, we see in Table II that the corrections with D for $r=1,2$ are $O(D^{-1})$. Indeed, the path counting arguments in Appendix A are plagued by corrections of $O(D^{-1})$.
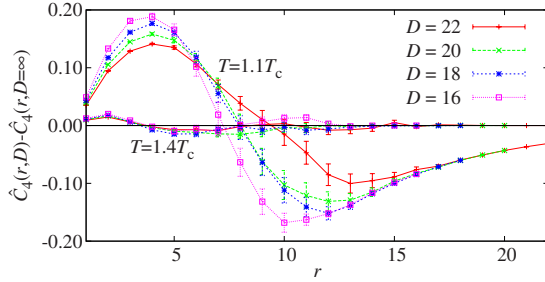
FIG. 7. (Color online) Difference between the numerical and analytical spatial correlation functions for different system sizes at two temperatures, $T=1.1T_c$ and $T=1.4T_c$.

B. SG phase

In the SG phase, our test has been restricted to a check of Eq. (2), which predicts a SG phase transition for the high-D limit. With this aim, we compute the Binder cumulant, $B(T)$, nearby T_c. For all $T < T_c$, we expect $B(T) < 3$ for large enough D. As we show in Fig. 8, $B(T)$ decreases with T and shows sizable finite size effects. In fact, at $T=0.99T_c$, we need to simulate lattices as large as $D=20$ to find values below 3. Right at T_c, the Gaussian value $B(T)=3$ is found for all the simulated sizes.

VI. NONEQUILIBRIUM RESULTS

In this section we will address the main features of the nonequilibrium dynamics obtained in our largest system, $D=22$. The issue of finite D corrections will be postponed to Sec. VII.

A. Structure of isothermal aging

The picture of isothermal aging dynamics in MF models of SG behavior was largely drawn in Ref. 30 (see also Ref. 31). The dynamics is ruled by an infinite number of *time sectors*,

$$C(t,t_w) = \sum_i f_i[h_i(t_w)/h_i(t+t_w)]. \quad (19)$$

The scaling functions f_i are positive, monotonically decreasing and normalized, i.e., $1 = \Sigma_i f_i(1)$. The unspecified functions h_i are such that, in the large t_w limit, $h_i(t_w)/h_i(t+t_w)$ is 1 if $t \ll t_w^{\mu_i}$, while it tends to zero if $t \gg t_w^{\mu_i}$. In other words, the
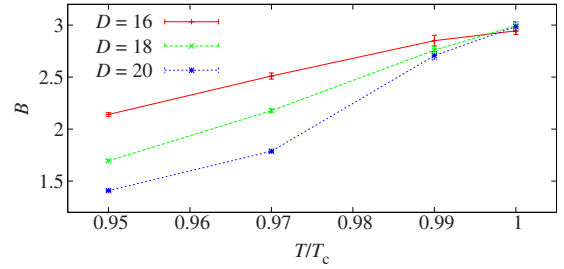

FIG. 8. (Color online) Equilibrium values of Binder cumulant (7) for several system sizes as a function of the temperature in units of the exact asymptotic value of T_c [Eq. (2)] in the SG phase.

decay of C between values C_i and C_{i+1} is ruled by the scaling function f_i and takes place in the time sector $t \sim t_w^{\mu_i}$.

This picture is radically different to the full aging often found both in experiments and in 3D simulations. A full aging dynamics is ruled only by two sectors of time, $\mu_i = 0, 1$. Nevertheless, recent experimental studies[4] show that full aging is no longer fulfilled for $t \gg t_w$. Probably more time sectors must be considered to rationalize these experiments.

However, Eq. (19) is probably an oversimplification since the spectrum of exponents μ_i might be continuous. An explicit realization of this idea was found in the critical dynamics of the trap model,[32] where the correlation function behaves for large t_w as

$$C(t,t_w) = f[\alpha(t,t_w)], \quad \alpha(t,t_w) = \log t/\log t_w. \quad (20)$$

Again, the scaling function f is positive and monotonically decreasing. Clearly enough, in the limit of large t_w and for any positive exponent μ, if $t = At_w^\mu$, the correlation function takes a value that depends only on μ no matter the value of the amplitude A.

As expected, $C(t,t_w)$ is clearly not a function of t/t_w in our model (see Fig. 9). On the contrary, data seem to tend to a constant value when $t_w \to \infty$ in any finite range of the variable t/t_w. This is precisely what one would expect in a time-sector scheme. On the other hand, if we try (without any supporting argument) the Bertin-Bouchaud (BB) scaling [Eq. (20); see Fig. 10], the data collapse is surprisingly good. Therefore, the nonequilibrium dynamics in the SG phase seems ruled by a, not only infinite but continuous, spectrum of time sectors.

We note *en passant* that scaling (20) is ultrametric only if the scaling function reaches a constant value for all $\alpha(t,t_w)$
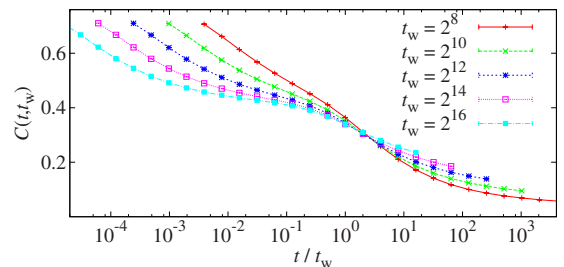
TABLE II. D times the difference between $\hat{C}_4(r)$ for finite D and infinite D as computed for $r=1,2$. The absence of any D evolution evidences finite-D corrections of order $1/D$.

	$r=1$		$r=2$	
D	$T=1.1T_c$	$T=1.4T_c$	$T=1.1T_c$	$T=1.4T_c$
16	0.783(6)	0.198(5)	2.130(18)	0.320(12)
18	0.779(4)	0.201(3)	2.115(11)	0.327(7)
20	0.784(2)	0.202(2)	2.109(6)	0.332(4)
22	0.7776(12)	0.2006(9)	2.083(4)	0.324(2)

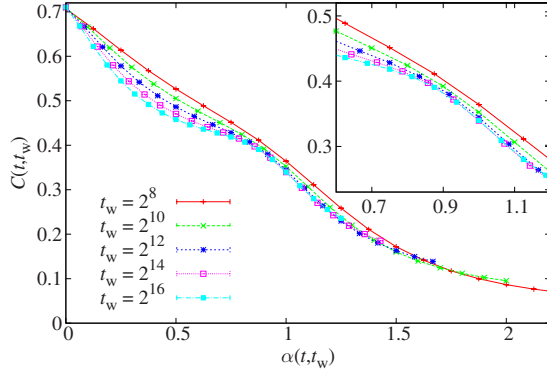FIG. 9. (Color online) $C(t,t_w)$ over t/t_w for $D=22$ and $T=0.7T_c$.

FIG. 10. (Color online) Same data of Fig. 9 as a function of $\alpha(t,t_\mathrm{w})$ defined in Eq. (20). The window is a zoomed image of the central region.

>1 (for details see Appendix B). In fact, dynamic ultrametricity is a geometric property[30] that states that for all triplet of times $t_1 \gg t_2 \gg t_3$, one has in the limit $t_3 \to \infty$,

$$C(t_1 - t_3, t_3) = \min\{C(t_1 - t_2, t_2), C(t_2 - t_3, t_3)\}. \quad (21)$$

Finding dynamical ultrametricity in concrete models has been rather elusive up to now. An outstanding example is the critical trap model,[32] where $f(\alpha > 1) = 0$. It is amusing that the trap model is *not* ultrametric from the point of view of the equilibrium states.[33] Thus, the casual connections between static and dynamic ultrametricities are unclear to us. At any rate, since our scaling function in Fig. 10 does not show any tendency to become constant for $\alpha(t,t_\mathrm{w}) > 1$, we do not find compelling evidences for dynamic ultrametricity in this model.

We have also looked directly to the plots of $C(t_1 - t_2, t_2)$ versus $C(t_2 - t_3, t_3)$ (see Appendix B) and we have not found convincing indications for the onset of dynamical ultrametricity. In this respect, it is worth recalling similarly inconclusive numerical investigations of the Sherrington-Kirkpatrick model.[30,34] There are two possible conclusions:

(1) the model does not satisfy dynamical ultrametricity in spite of the fact that it satisfies (according to the standard wisdom) static ultrametricity or

(2) dynamical ultrametricity holds, but its onset is terribly slow.

Both conclusions imply that it is rather difficult to use the dynamic experimental data (or any kind of data) to get conclusions on static ultrametricity. Of course it would be cru-
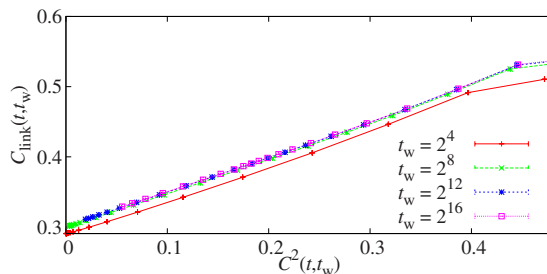

FIG. 11. (Color online) C_link over $C^2(t,t_\mathrm{w})$ for different t_w at $T = 0.7T_\mathrm{c}$ and for $D = 22$.

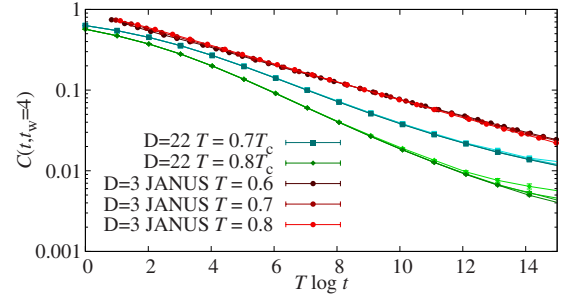
FIG. 12. (Color online) Thermoremanent magnetization over $T \log t$. The JANUS data (in red circles) follow a power law with an exponent $\propto 1/T$. Our results for $D = 22$ are shown in dark tonalities (lighter colors: $D < 22$).

cial to check if static ultrametricity is satisfied in this model, but this is beyond the scope of this paper.

B. Aging in C_link

Just as in the 3D case,[7] the aging dynamics in SGs in the hypercube is a domain-growth process (see Fig. 17). For any such process, the question of the surface-volume ratio arises. When this ratio vanishes in the limit of large domain size, as it is the case for any RSB dynamics, one expects a linear relation between $C_\mathrm{link}(t,t_\mathrm{w})$ and $C^2(t,t_\mathrm{w})$. This is precisely what we find in Fig. 11.

C. Thermoremanent magnetization

The experimental work indicates that for $T < 0.9T_\mathrm{c}$, the thermoremanent magnetization follows a power law with an exponent proportional to T_c/T.[35] The data obtained in JANUS for a three-dimensional SGs (see Fig. 12 and Ref. 28) agree with this statement. However, the data obtained in the hypercube model do not follow such power law, neither can be rescaled with $T \log t$.

This lack of an algebraic decay is surprising on the view of the exact results in Ref. 36. Indeed, it was analytically shown there that, at T_c, the thermoremanent magnetization of
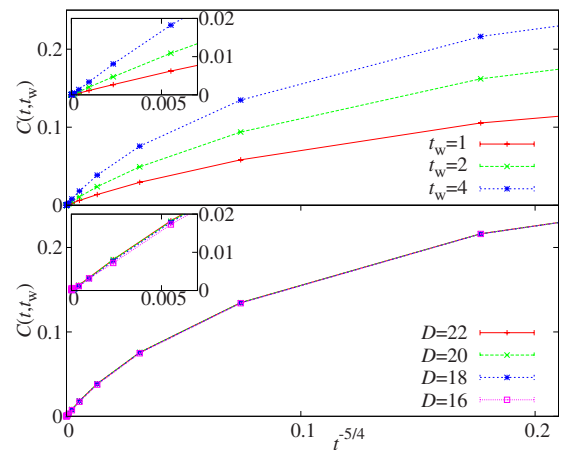

FIG. 13. (Color online) Thermoremanent magnetization at T_c vs $t^{-5/4}$ for (up) different t_w and $D = 22$ and (down) different system sizes for $t_\mathrm{w} = 4$. The two insets are the closeups of the origin.
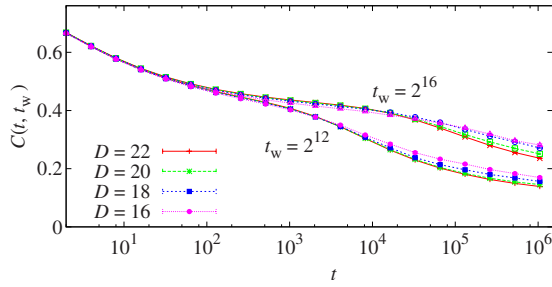
FIG. 14. (Color online) Finite size effects in $C(t,t_{\rm w})$ at $T = 0.7T_{\rm c}$.

FIG. 16. (Color online) $C_{\rm link}$ over $C^2(t,t_{\rm w})$ at $T = 0.7T_{\rm c}$ for $t_{\rm w} = 2^{12}$ and for different system sizes.

the SK model decays as $t^{-5/4}$. Universality strongly suggests that the same scaling should hold for our model. Although it seems not to be the case, at the first glance (Fig. 13, top), a closer inspection confirms our expectation. Indeed, when plotted as a function of $t^{-5/4}$ (see the inset of Fig. 13, top), the thermoremanent magnetization curve has a finite nonvanishing slope at the origin. As we show in bottom panel of Fig. 13, finite size effects do not contradict this claim. In summary, the magnetization decay for the hypercube suffers from quite strong finite time effects, but asymptotically it scales with the proper exponent, at least at $T_{\rm c}$.

VII. NONEQUILIBRIUM CORRELATION FUNCTIONS AND FINITE SIZE EFFECTS

The importance of finite size effects in nonequilibrium dynamics has been emphasized recently.[7,28] In our case, we have encountered important size effects both in $C(t,t_{\rm w})$ (Fig. 14) and in $\xi(t_{\rm w})$ (Fig. 17, top).

We compare in Fig. 15 the finite D effects in $C(t,t_{\rm w})$ for two different MF models with fixed connectivity: the hypercube and a previously studied model (the random graph with connectivity $z = 6$, where each spin can interact with any other spin with uniform probability[37]). Clearly enough, the effects are much weaker in the hypercube model.

It is interesting to point out that, although the finite size effects seem to be important in $C(t,t_{\rm w})$, they are largely absorbed when one eliminates the variable t in favor of $C^2(t,t_{\rm w})$ (see Fig. 16). Hence, one of our main findings (the linear behavior of $C_{\rm link}$ as a function of C^2) seems not endangered by finite size effects.

A very clear finite size effect is in the coherence length, $\xi(t_{\rm w})$. By definition, it cannot grow beyond D. Furthermore,
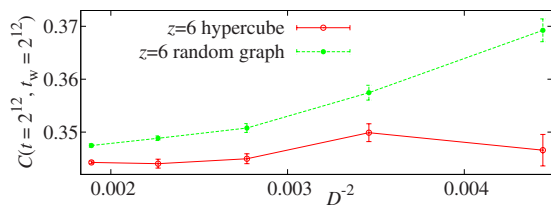

FIG. 15. (Color online) $C(t,t_{\rm w})$ at $T = 0.7T_{\rm c}$ for $t = t_{\rm w} = 2^{12}$ vs $1/D^2$. We compare results obtained with two $z = 6$ models: one with hypercubic topology (red open circles) and another in a totally random graph (green full circles).
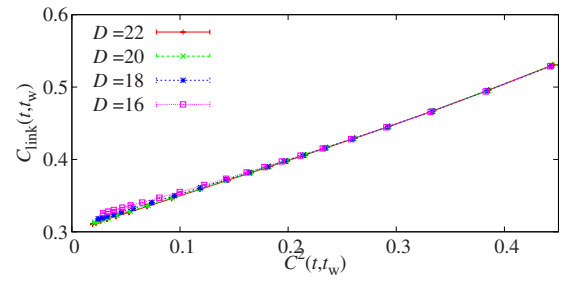
what we find is that it hardly grows beyond $D/2$ (Fig. 17, top). Nevertheless, at short times, we can identify a D-independent region, where it grows roughly as $\log t_{\rm w}$. Hence, one is tempted to conclude that $\xi_{D=\infty}(t_{\rm w}) \propto \log t_{\rm w}$. At this point, finite size scaling suggests that both ξ_D/D and $\log t_{\rm w}/D$ are dimensionless scaling variables. This is confirmed in Fig. 17 (bottom), where a spectacular data collapse occurs. This is further confirmed by the Fourier transform $G(k)$, defined in Eq. (17). Now, since k can range from 0 to D, it is clearly a dimensionless quantity (a dimensionful momentum would be $p = k/D$). It follows that $G(k)/G(0)$ is a dimensionless quantity that may depend only on a dimensionless variable, such as $\log t_{\rm w}/D$. Our data support this expectation (see Fig. 18).

As for the k dependence of $G(k)$, we expect a $1/p^4$ behavior in the range of $1/\xi(t_{\rm w}) \ll p \ll 1$.[16] Indeed, when comparing nonequilibrium with equilibrium spatial correlation functions, it should be kept in mind that the nonequilibrium ones correspond to the equilibrium $q = 0$ sector[7,8] (since we take the large D limit at fixed $t_{\rm w}$).

Now, it is very important to recall that p^4 in Euclidean metrics translates into p^2 in the postman metrics. We have also seen that the dimensionful p (postman metrics) corresponds to k/D. Thus, since in our range of $t_{\rm w}$ $\xi(t_{\rm w}) \sim \log t_{\rm w}$, the product $G(k)(p^2 + 1/\log^2 t_{\rm w})$ should be roughly constant as D grows. As we show in Fig. 19, the scaling is better for p of order 1 ($k \sim D$), although it seems to improve for smaller p as D grows. We remark the importance of observing a p^4 propagator in a numerical work.
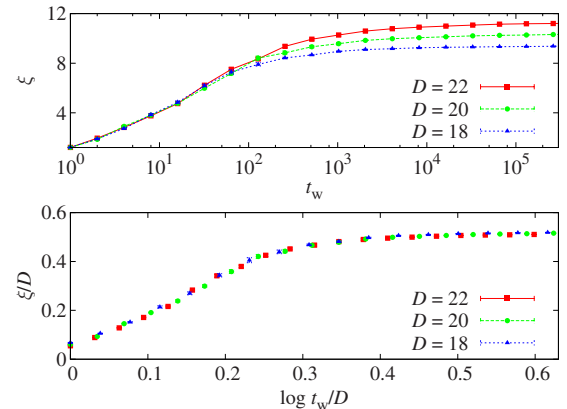

FIG. 17. (Color online) (Top) Coherence length ξ in the SG phase at $T = 0.7T_{\rm c}$ vs $t_{\rm w}$ for different system sizes. (Bottom) Same data of the top panel rescaled by D as a function of $\log t_{\rm w}/D$.
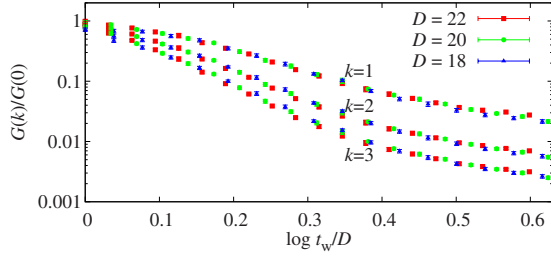
FIG. 18. (Color online) Fourier transform $G(k)$ of $\hat{C}_4(r)$ in units of $G(0)$ as a function of $\log t_{\rm w}/D$ for several values of D and k at $T = 0.7T_{\rm c}$. For each value of k, a different scaling function is found.

VIII. CONCLUSIONS

We have studied a spin-glass model in the D-dimensional unit hypercube in the limit of large D but with finite coordination number. We have shown that any short range model in such a lattice will behave as a mean field model in the thermodynamic limit (that coincides with the large D limit). An important advantage of this model is that it has a natural notion of spatial distance.

We have argued that any statistical mechanics model on the hypercube with random connectivity would be afflicted by huge finite size effects for purely geometrical reasons. The obvious cure has consisted in restricting the connectivity graphs to those with a fixed number of neighbors. Unfortunately, constructing such graphs is far from trivial. We have generated a subset of them by means of a simple dynamic Monte Carlo. In this way, we obtain graphs that are isotropic. We have checked that the Edwards-Anderson model defined over these finite connectivity hypercubes verifies some consistency checks, including comparison with the analytically computable correlation function in the paramagnetic phase.

We have numerically studied the nonequilibrium dynamics in the spin-glass phase. The three main features found were the following: (i) aging dynamics consists of the growth of a coherence length, much as in 3D systems, (ii) the
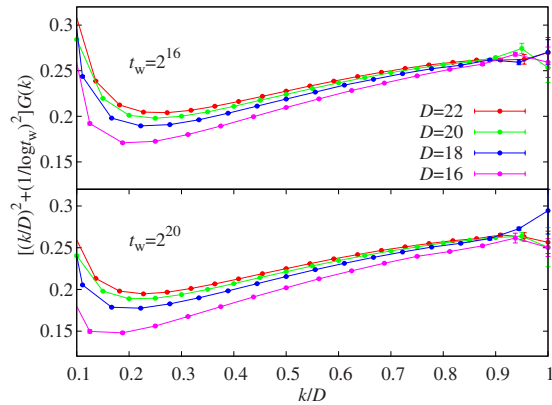

FIG. 19. (Color online) Fourier transform $G(k)$ [Eq. (17)] in units of the propagator $\{[p^2 + 1/\xi^2(t_{\rm w})]^{-1}\}$ (Ref. 16) as a function of p, where the dimensionful momentum is $p = k/D$ and $\xi(t_{\rm w}) \sim \log t_{\rm w}$. Recall that we are using postman metrics, hence, p^2 translates to p^4 in the Euclidean metrics. We show results for two waiting times: $t_{\rm w} = 2^{16}$ (top) and $t_{\rm w} = 2^{20}$ (bottom).

scaling of the two-time correlation function implies infinitely many time sectors, and (iii) the p^4 propagator has been observed. In addition, we have studied the finite size effects in our model, finding that a naive finite size scaling ansatz accounts for our data.

From the static point of view, it is most probable, almost a theorem, that our model suffers replica symmetry breaking. Hence, it provides an interesting playground to study nonequilibrium dynamics on RSB systems. An interesting possible extension of the present study would be the computation of quantities that are directly measurable in experiments and/or of experimental cooling protocols.

APPENDIX A: HIGH TEMPERATURE EXPANSION

For the sake of clarity, we will first discuss the calculations for the random-connectivity hypercube. Results for the fixed connectivity model will be then obtained by minor changes.

Using the identity ($\beta = 1/T$)

$$e^{\beta J_{xy}\sigma_x\sigma_y} = \cosh\beta(1 + J_{xy}\sigma_x\sigma_y \tanh\beta), \quad (A1)$$

we can write the partition function and the spin propagator as (N_l is the total number of links in the graph)

$$\frac{Z}{2^N(\cosh\beta)^{N_l}} = \sum_{\{\sigma\}}\prod_{\langle zw\rangle}(1 + J_{zw}\sigma_z\sigma_w \tanh\beta),$$

$$\langle\sigma_x\sigma_y\rangle = \frac{\displaystyle\sum_{\{\sigma\}}\sigma_x\sigma_y\prod_{\langle zw\rangle}(1 + J_{zw}\sigma_z\sigma_w \tanh\beta)}{\displaystyle\sum_{\{\sigma\}}\prod_{\langle zw\rangle}(1 + J_{zw}\sigma_z\sigma_w \tanh\beta)}. \quad (A2)$$

The high-temperature expansion (see, for instance, Ref. 38) expresses the propagator as a sum over lattice paths that join the points x and y, $\gamma_{x\to y}$,

$$\langle\sigma_x\sigma_y\rangle = Z^{-1}\sum_{\gamma_{x\to y}} Z_\gamma J(\tanh\beta)^{l_\gamma}, \quad (A3)$$

where l_γ represents the length of the path $\gamma_{x\to y}$, J is the product of the couplings, J_{zw}, along the path, and Z_γ is a restricted partition function obtained by summing only over all closed paths that do not have any common link with the path $\gamma_{x\to y}$.

However, when averaging over disorder, due to the randomness in the coupling signs, $\overline{\langle\sigma_x\sigma_y\rangle} = 0$. The spin-glass propagator is obtained instead by averaging over disorder $\overline{\langle\sigma_x\sigma_y\rangle^2}$. Clearly, the sum will be dominated by those dia-

grams where the go and return paths are the same (thus, $\bar{J}_{zw}^2 = 1$),

$$\overline{\langle \sigma_x \sigma_y \rangle^2} = Z^{-2} \sum_{\gamma_{x \to y}} Z_\gamma^2 [\tanh^2 \beta]^{l_\gamma} = Z^{-2} \sum_{\gamma_{x \to y}} K^{l_\gamma} Z_\gamma^2, \tag{A4}$$

where $K = \tanh^2 \beta$. In the Bethe lattices, due to their cycleless nature, $Z_\gamma^2 / Z^2 = 1$ in the thermodynamic limit. Hence, we are left with the problem of counting the average number of paths of length l_γ that join x and y, $p(l_\gamma)$. From it, we obtain

$$\hat{C}_4(r) = \binom{D}{r} \sum_{l_\gamma \geq r} p(l_\gamma) K^{l_\gamma}. \tag{A5}$$

The sum is restricted to $l_\gamma \geq r$ because the length of the shortest path that joins x and y is given by their postman distance r.

In order to count the average number of paths, $p(l_\gamma)$, let us distinguish two cases: $l_\gamma = r$ and $l_\gamma > r$. The first will give the leading contribution in the large D limit.

The number of paths joining x and y in precisely r steps is $r!$ because the r steps are all taken along different directions and in a random order. For a given path, the probability of all the r links being active is $(z/D)^r$. Hence

$$p(l_\gamma = r) = \frac{z^r}{D^r} r!. \tag{A6}$$

Note that the D^{-r} factor compensates exactly the divergence of the $\binom{D}{r}$ in Eq. (A5).

In the case of $l_\gamma > r$, one has $l_\gamma = r + 2k$, with $k > 0$. Note that when $l_\gamma = r$ the path contains r different directions (namely, the Euclidean components in which x and y differ). Each of these directions appear only once. However, when $l_\gamma > r$, other directions must be included; we call them unnecessary. Note that, if the path is to end at the desired point, any unnecessary step must be undone later on. Hence, $l_\gamma - r$ is always an even number $2k$. Clearly, the number of such paths is bounded by $\Gamma(r,k) D^k$, where $\Gamma(r,k)$ is a D-independent amplitude. On the other hand, the probability of finding all the links active is $(z/D)^{r+2k}$. Thus, we conclude that

$$p(l_\gamma = r + 2k) = O\left(\frac{1}{D^{k+r}}\right), \tag{A7}$$

which results in a $O(D^{-k})$ contribution to $\hat{C}_4(r)$.

Then, in the large D limit we obtain $(A = zK)$,

$$\hat{C}_4(r) = A^r = e^{r \log A}, \tag{A8}$$

with finite size corrections of $O(D^{-1})$. Thus, we encounter an exponential decay with an exponential correlation length given by

$$\xi^{\text{exp}} = \frac{1}{|\log A|}. \tag{A9}$$

Summing all up, we can compute the spin-glass susceptibility for the large D limit,

$$\chi = \sum_{r=0}^\infty \hat{C}_4(r) = \sum_{r=0}^\infty A^r = \frac{1}{1-A}. \tag{A10}$$

We see that when $A = 1$ the correlation no longer decays with distance and the susceptibility diverges. Of course, one gets $A = 1$ precisely at the critical temperature, T_c, reported in Eq. (2).

The computation for the fixed connectivity model is very similar. One only needs to notice that, whereas the probability for the first link in a lattice path to be active is z/D, the probability for the next link is roughly $(z-1)/D$ (this is only accurate for large D). It follows that, again, the $l_\gamma = r$ paths are the only relevant paths in the high-temperature expansion. We find that

$$p(l_\gamma = r) = \begin{cases} 1 & \text{if } r = 0 \\ \dfrac{z}{D}\left(\dfrac{z-1}{D}\right)^{r-1} r! & \text{if } r > 0. \end{cases} \tag{A11}$$

Again, we can use it to compute $\hat{C}_4(r)$. In the large D limit, up to corrections of $O(D^{-1})$, it is given by

$$\hat{C}_4(r) = \begin{cases} 1 & \text{if } r = 0 \\ \dfrac{z}{z-1}[(z-1)K]^r & \text{if } r > 0, \end{cases} \tag{A12}$$

which, taking $\tilde{A} = (z-1)K$, also shows an exponential decay with

$$\xi^{\text{exp}} = \frac{1}{|\log \tilde{A}|}. \tag{A13}$$

Using this spatial correlation function, we can either compute the SG susceptibility in the fixed connectivity hypercube,

$$\chi = \sum_{r=0}^\infty \hat{C}_4(r) = 1 + \frac{z}{z-1} \frac{\tilde{A}}{1-\tilde{A}}, \tag{A14}$$

or the integral correlation length, defined as Eq. (13),

$$\xi = \frac{\displaystyle\sum_{r=0}^\infty r \hat{C}_4(r)}{\displaystyle\sum_{r=0}^\infty \hat{C}_4(r)} = \frac{\chi - 1}{\chi} \frac{1}{1-\tilde{A}}. \tag{A15}$$

Again, when $\tilde{A} = 1$, we find a critical point. The corresponding T_c matches Eq. (2). The critical exponents, $\gamma = 1$, $\nu = 1$, can be read directly from Eqs. (A14) and (A15). The reader might be puzzled by a mean field model with $\nu \neq 1/2$. The solution to the paradox is in our chosen metrics. Recall that the postman distance in the hypercube is the square of the Euclidean one. Hence, the correlation length in Eq. (A15) is the square of the Euclidean correlation length.

APPENDIX B: SCALING AND DYNAMIC ULTRAMETRICITY

As in Eq. (20), let us assume that the spin time correlation function behaves for large t_w as

$$C(t,t_w) = f[\alpha(t,t_w)], \quad \alpha(t,t_w) = \log t / \log t_w, \quad \text{(B1)}$$

where the scaling function f is smooth and monotonically decreasing. From now on, we shall refer to this scaling as BB scaling (after Bertin-Bouchaud).

Let us see under which conditions BB scaling implies the ultrametricity property,

$$C(t_1 - t_3, t_3) = \min\{C(t_1 - t_2, t_2), C(t_2 - t_3, t_3)\}, \quad \text{(B2)}$$

where $t_1 \gg t_2 \gg t_3$ and t_3 tends to infinity.

The natural time dependency is a power-law choice,

$$t_1 = t_3 + A t_3^{\mu_1}, \quad \text{(B3)}$$

$$t_2 = t_3 + B t_3^{\mu_2}, \quad \text{(B4)}$$

with $\mu_1 > \mu_2$. In that case, the large t_3 limits for the argument of the scaling function are $\alpha(t_1 - t_3, t_3) = \mu_1$, $\alpha(t_2 - t_3, t_3) = \mu_2$, and $\alpha(t_1 - t_2, t_2) = \mu_1$ if $\mu_2 < 1$ and $\alpha(t_1 - t_2, t_2) = \mu_1/\mu_2$ if $\mu_2 > 1$. Then, condition (B2) is only satisfied in case $\mu_2 < 1$. If, as it is the case for the critical trap model,[32] $f(\alpha > 1)$ =const,[39] the BB scaling would imply dynamic ultrametricity. This is not the case for a general scaling function f such as, for instance, the one we get in Fig. 10. Nevertheless, although this analysis implies that the dynamic ultrametricity
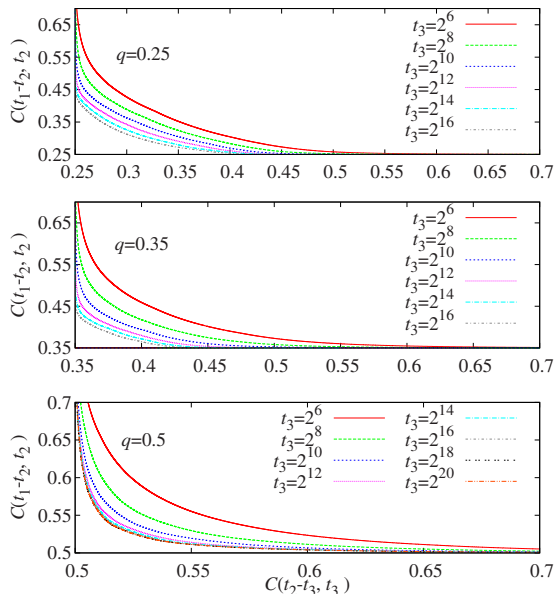

FIG. 20. (Color online) Parametric plot $[x(t_2), y(t_2)] = [C(t_1 - t_2, t_2), C(t_2 - t_3, t_3)]$, $t_1 > t_2 > t_3$ with t_1 fixed by the condition $C(t_1 - t_3, t_3) = q$ and different t_3. In the presence of dynamic ultrametricity (B2), the parametric plot should tend for large t_3 to the union of $x = q$ and $y = q$. The panels correspond to $q = 0.25$ (top, nice BB scaling but no ultrametricity expected), $q = 0.35$ (middle, nice BB scaling and ultrametricity expected), and $q = 0.5$ (bottom, supposedly ultrametric but poor BB scaling). Note that there are not qualitative differences between $q = 0.25$ and $q = 0.35$.
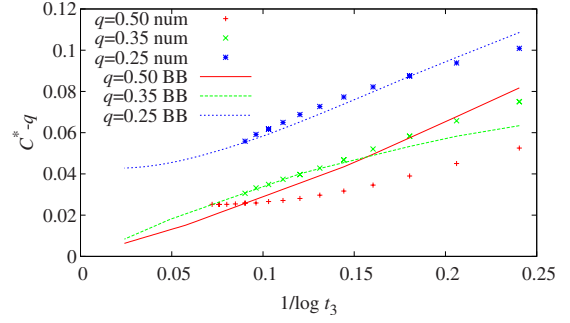

FIG. 21. (Color online) Dots: for each q and t_3, as in Fig. 20, we take the intercept with $x = y$, i.e., $C^* = C(t_1 - t_2, t_2) = C(t_2 - t_3, t_3)$, and represent $C^* - q$ as a function of $1/\log t_3$. Lines: analogous plot for the toy model described in the text, where the BB scaling is exact.

is only present in our model in some range of parameters, let us try a more straight approach.

We consider a fixed value for the correlation function, q. On the view of the previous considerations and of Fig. 10, we should expect ultrametricity only for $q > f(\alpha = 1) \approx 0.35$. Now, for each t_3, we find t_1 such that $C(t_1 - t_3, t_3) = q$. Then, we perform a parametric plot of $C(t_1 - t_2, t_2)$ vs $C(t_2 - t_3, t_3)$ for $t_3 < t_2 < t_1$. Ultrametricity predicts that, in the large t_3 limit, the curves should tend to a half square (e.g., the intersection of the straight lines $x = q$ and $y = q$) and, in particular, when $C(t_1 - t_2, t_2) = C(t_2 - t_3, t_3) = C^*$, C^* should tend to q.

We present in Fig. 20 results for three different values of q: 0.5 (ultrametric region but in our range of t_w data do not scale according to BB), 0.35 (ultrametric region and good BB scaling), and 0.25 (nonultrametric region but BB scaling works nicely). At the qualitative level, the parametric curves seem to tend to a corner (but $q = 0.5$), but the convergence is slow. Furthermore, there are no clear differences between the curves with $q > f(\alpha = 1)$ and those with $q < f(\alpha = 1)$. Hence, due to the failure of this qualitative approach, we may try a more quantitative analysis.

We obtain numerically C^*, the point where $C^* = C(t_1 - t_2, t_2) = C(t_2 - t_3, t_3)$, and study $C^* - q$ as function of $1/\log t_3$. This choice is due to the fact that in the ultrametric region BB scaling predicts

$$\alpha(t_1 - t_2, t_2) = \alpha(t_1 - t_3, t_3) - \frac{\log 2}{\log t_3} + \cdots. \quad \text{(B5)}$$

Hence, we expect that $C^* - q$ will be of order $1/\log t_3$ if ultrametricity holds. Let us sketch the proof. We define $y = f^{-1}(q) = \alpha(t_1 - t_3, t_3)$ (recall that $y < 1$ in the ultrametric region). Hence, the three times are

$$t_1 = t_w + t_w^y, \quad \text{(B6)}$$

$$t_2 = t_w + A(t_w) t_w^y, \quad \text{(B7)}$$

$$t_3 = t_w. \quad \text{(B8)}$$

The hierarchy of time scales, $t_1 > t_2 > t_3 \gg 1$, implies that, for

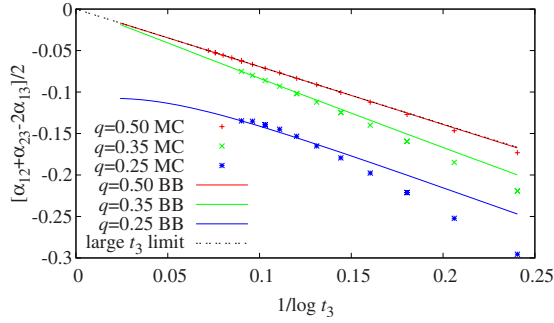FIG. 22. (Color online) For the data in Fig. 21, we represent $[\alpha(t_1,t_2)+\alpha(t_2,t_3)]/2-\alpha(t_1,t_3)$ vs $1/\log t_3$. The dashed line corresponds to Eq. (B5).

large t_w, $A(t_w)$ is bounded. The condition $\alpha(t_1-t_2,t_2)=\alpha(t_2-t_3,t_3)$ translates to

$$\frac{y\log t_w+\log[1-A(t_w)]}{\log t_w+\log[1+A(t_w)t_w^{y-1}]}=y+\frac{\log A(t_w)}{\log t_w}. \qquad \text{(B9)}$$

The above equation can be solved asymptotically for $A(t_w)$ in the limit of large t_w as (recall that $y<1$)

$$A(t_w)=\frac{1}{2}-\frac{y}{8}t_w^{y-1}+\cdots. \qquad \text{(B10)}$$

To obtain Eq. (B5), one just notes that $\alpha(t_1-t_2,t_2)$ is equal to the right-hand side of Eq. (B9).

The MC numerical data in Fig. 21 confirm the expectation of $C^*-q=O(1/\log t_3)$ only partly. For $q=0.35$ the results are as expected, yet for $q=0.25$ the difference is decreasing fast as t_3 grows and it is hard to tell whether the extrapolation will be zero or not. For $q=0.5$ (where BB scaling is not working for our numerical data) the behavior is nonmonotonic.

To rationalize our finding, we consider a simplified model, where the BB scaling is supposed to hold exactly. The master curve $f(\alpha)$ is taken from the numerical data for $C(t,t_3=2^{16})$ for $D=22$. This toy model allows us to consider ridiculously large values of t_3. As we see in Fig. 21, the peculiarities of the master curve cause a nonmonotonic behavior in q for an ample range of t_3.

The lack of monotonicity in q makes also on interest to focus on α rather than on the correlation function. With this aim, we consider the time t_2 where $C(t_1-t_2,t_2)=C(t_2-t_3,t_3)=C^*$ and compute $\frac{1}{2}[\alpha(t_1-t_2,t_2)+\alpha(t_2-t_3,t_3)]-\alpha(t_1-t_3,t_3)$. BB scaling and ultrametricity combined [see Eq. (B5)] imply that this quantity should be of order $1/\log t_3$ (in the nonultrametric region, it should be of order 1). Our results in Fig. 22 basically agree with these expectations.

[1] J. A. Mydosh, *Spin Glasses: An Experimental Introduction* (Taylor & Francis, London, 1993).

[2] K. Jonason, E. Vincent, J. Hammann, J. P. Bouchaud, and P. Nordblad, Phys. Rev. Lett. **81**, 3243 (1998).

[3] G. F. Rodriguez, G. G. Kenning, and R. Orbach, Phys. Rev. Lett. **91**, 037203 (2003).

[4] G. G. Kenning, G. F. Rodriguez, and R. Orbach, Phys. Rev. Lett. **97**, 057201 (2006).

[5] K. Gunnarsson, P. Svedlindh, P. Nordblad, L. Lundgren, H. Aruga, and A. Ito, Phys. Rev. B **43**, 8199 (1991).

[6] S. Franz, M. Mézard, G. Parisi, and L. Peliti, Phys. Rev. Lett. **81**, 1758 (1998); J. Stat. Phys. **97**, 459 (1999).

[7] F. Belletti, M. Cotallo, A. Cruz, L. A. Fernandez, A. Gordillo-Guerrero, M. Guidetti, A. Maiorano, F. Mantovani, E. Marinari, V. Martin-Mayor, A. M. Sudupe, D. Navarro, G. Parisi, S. Perez-Gaviro, J. J. Ruiz-Lorenzo, S. F. Schifano, D. Sciretti, A. Tarancon, R. Tripiccione, J. L. Velasco, and D. Yllanes, Phys. Rev. Lett. **101**, 157201 (2008).

[8] R. Alvarez Baños *et al.*, JANUS collaboration, arXiv:1003.2569.

[9] D. S. Fisher and D. A. Huse, Phys. Rev. Lett. **56**, 1601 (1986); Phys. Rev. B **38**, 386 (1988).

[10] E. Marinari, G. Parisi, F. Ricci-Tersenghi, J. J. Ruiz-Lorenzo, and F. Zuliani, J. Stat. Phys. **98**, 973 (2000).

[11] D. S. Fisher and D. A. Huse, Phys. Rev. B **38**, 373 (1988).

[12] F. Krzakala and O. C. Martin, Phys. Rev. Lett. **85**, 3013 (2000); M. Palassini and A. P. Young, *ibid.* **85**, 3017 (2000).

[13] D. Sherrington and S. Kirkpatrick, Phys. Rev. Lett. **35**, 1792 (1975).

[14] M. Mézard and G. Parisi, Eur. Phys. J. B **20**, 217 (2001).

[15] A nondiluted spin glass model on a D-dimensional hypercube, in the limit of large D, was considered by G. Parisi, F. Ritort, and J. M. Rubi, J. Phys. A (Math. Gen.) **24**, 5307 (1991), while a fully frustrated model was studied by E. Marinari, G. Parisi, and F. Ritort, *ibid.* **28**, 327 (1995).

[16] C. De Dominicis, I. Kondor, and T. Temesvari, Int. J. Mod. Phys. B **7**, 986 (1993); *Spin Glasses and Random Fields*, edited by P. Young (World Scientific, Singapore, 1997); C. De Dominicis and I. Giardina, *Random Fields and Spin Glasses: A Field Theory Approach* (Cambridge University Press, Cambridge, 2006).

[17] G. Parisi, Proceedings of the 2006 Les Houches Summer School (unpublished).

[18] D. J. Thouless, Phys. Rev. Lett. **56**, 1082 (1986).

[19] F. Ricci-Tersenghi, private communication.

[20] This movement keeps each vertex connectivity unaltered. Besides, a transformation and its opposite are equally probable. As a consequence the detailed balance condition is satisfied with respect to the uniform measure on the ensemble of fixed connectivity graphs. A standard theorem[23] ensures that the equilibrium state of this Markov chain is the uniform measure over the subset of fixed connectivity hypercubes reachable from the initial condition by means of plaquette transformations.

[21] We use a very simple algorithm to find the length of the second shortest path joining two neighboring spins i_1, i_2. We consider a truncated connectivity matrix, $\tilde{n}$, which coincides with the true one, n, but for the link i_1-i_2, which is deactivated: $\tilde{n}_{i_1,i_2}=\tilde{n}_{i_2,i_1}=0$. We take a starting vector $v^{(0)}$ with all its components set to 0 but the component i_1 is set to 1. We iteratively multiply the

vector by the truncated connectivity matrix, i.e., $\boldsymbol{v}^{(t)} = \widetilde{n}\boldsymbol{v}^{(t-1)}$, until the i_2th component is nonzero. The sought length is just the minimum value of t that fulfills the stopping condition.

[22] We say that a graph is a tree-graph if, once the link between two neighboring spins is removed, there is no way of joining them following any other path.

[23] See, e.g., D. J. Amit and V. Martin-Mayor, *Field Theory: The Renormalization Group and Critical Phenomena*, 3rd ed. (World Scientific, Singapore, 2005).

[24] M. Hasenbusch, A. Pelissetto, and E. Vicari, Phys. Rev. B **78**, 214205 (2008).

[25] We store configurations at times $2^n + 2^m$, with n,m integers. We calculate the correlation function for all (t, t_w) with power of 2, allowed by the simulation length.

[26] In the SG phase this is true only for $t \ll t_w$ (Ref. 31).

[27] Using gauge transformation (3), it is possible to rewrite an ordered configuration (by an external magnetic field, for instance) as the spin configuration found at time t_w after a random start.

[28] JANUS Collaboration, J. Stat. Phys. **135**, 1121 (2009).

[29] G. Parisi and F. Zamponi, J. Stat. Phys. **123**, 1145 (2006).

[30] L. F. Cugliandolo and J. Kurchan, J. Phys. A **27**, 5749 (1994).

[31] J. P. Bouchaud, L. Cugliandolo, J. Kurchan, and M. Mèzard, in *Spin Glasses and Random Fields*, edited by P. Young (World Scientific, Singapore, 1997).

[32] E. Bertin and J. P. Boucheaud, J. Phys. A **35**, 3039 (2002).

[33] M. Mèzard, G. Parisi, and M. Virasoro, *Spin Glass Theory and Beyond* (World Scientific, Singapore, 1987).

[34] L. Berthier, J. L. Barrat, and J. Kurchan, Phys. Rev. E **63**, 016105 (2000).

[35] P. Granberg, P. Svedlindh, P. Nordblad, L. Lundgren, and H. S. Chen, Phys. Rev. B **35**, 2075 (1987); J. J. Préjean and J. Souletie, *ibid.* **37**, 577 (1988), and references therein.

[36] G. Parisi, P. Ranieri, F. Ricci-Tersenghi, and J. J. Ruiz-Lorenzo, J. Phys. A **30**, 7115 (1997).

[37] L. Leuzzi, G. Parisi, F. Ricci-Tersenghi, and J. J. Ruiz-Lorenzo, Phys. Rev. Lett. **101**, 107203 (2008).

[38] G. Parisi, *Statistical Field Theory* (Addison-Wesley, Reading, MA, 1988).

[39] Weak ergodicity breaking implies that $f(\alpha > 1) = 0$.